Waves and Oscillations in the Solar Corona

First Year Progress Report

Ding Yuan

Supervisor: Professor Valery Nakariakov

April 15, 2010

Abstract

A progress report is summaried about the research background and on-going project after 6 months work. Our research on MHD waves and oscillation in the solar corona is covered in general format, headed with the motivation on the research and main challenges in the field as Section 1, a specialized subsection is delivered to modern instruments (Section 1.1), which are used in the research. This is followed by a instroduction to solar corona (Section 2), with the main objects that willl be encountered in the context almost in any solar research and publication. Then, the plasma theory about the waves and oscillations (Section 3) is given in general formulary, which is the basic and the theoretical source to explain other wave related issues in the astro or fusion plasma. A more specified cylinderial model based on the wave theory (Section 4) is briefed and leads to the theory of propagating slow-mode MHD waves and its observations and research methodology (Section5). Current project (Section 6) is summaried including the preliminary results, finally the future plan (Section7) is proposed till the Dec 2010. The five key texts are reviewed and added as appendice.

Contents

1 Motivation **4**
1.1 Modern Instruments 4

2 Solar Corona **5**
2.1 Active Region 6
2.2 Coronal Loops 6
2.3 Solar Plume 6
2.4 Prominence 6

3 Waves and Oscillations in the Plasma **6**

4 Standard Model: Straght Plasma Cylinder **8**

5 Propagatingclearly Perturbation of Intensity **9**

6 Current Projects **11**

7 Future Plan **15**
7.1 Shot Term Plan: April - June 2010 15
7.2 Long Term Plan: July - December 2010 15
7.3 Year 2 and 3 17

Appendices **19**

A Nakariakov and Verwichte (2005) **19**

B De Moortel (2009) **20**

C Torrence and Compo (1998) **21**

D Scargle (1982) **22**

E DeForest and Gurman (1998) **22**

1 Motivation

The shining sun is maintained by the nuclear fusion, the temperature at its core reaches more than 15MK and drops to around 6000K at the surface, however, the solar corona, aka, the solar upper atmosphere, made of full ionized gases, is amazingly hotter at temperature up to several MK. The physics of solar corona heating has been puzzled the scientist for decades, current advances identify two main candidates as explanations to the dilemma of corona heating: *magnetic reconnection theory* and *wave heating*. The latter is our main research area, furthermore, it introduces corona seismology techniques to remotely diagnose the parameters of the corona, *e.g.* , magnetic fields, transport coefficients, fine structuring and heating functions *etc.*

The magnetic reconnection theory based on the fact that, the magnetic field lines reconnect at the magnetic null points and induce electric current, then the electric currents collapse and dissipate the energy in forms of heat and waves in the corona. These process is hypothesized to be the mechanism behind solar flare, as the surface of the sun is covered by millions of small magnetized regions or magnetic carpets that under constant granulation. The motions of the magnetic carpets trigger the reconnection process and release the energy in a series of micro-flares to heat the corona.

In the wave heating theory, the waves, which can be generated by granulation and supergranulation at photosphere, carry energy from solar interior, propagate to the chromosphere and corona, the energy is dissipated and heat the corona up to millions of Kelvin. The most important types of waves are magnetic-acoustic wave and Alfvén wave. The issue is that, the magnetic-acoustic waves cannot carry enough energy due to the low pressure at chromosphere and easy reflection back to the photosphere; Alfvén waves carry enough energy, however, the energy couldn't be dissipated efficiently. Thus other physics is raised to complement the theory, *e.g.* resonant absorption, Alfvén wave mixing *etc.*

The coronal seismology techniques incorporate observations, MHD wave theory for remote diagnostics of the physical parameters of the solar or stellar corona. Based on the measurements, the properties of MHD waves and oscillations, *e.g.* period, damping factor, amplitude *etc.* In combination of MHD wave theory, the physical parameters of the corona ,*e.g.* magnetic fields, dissipative coefficients, sub-structuring *etc.* can be estimated with confidence.

1.1 Modern Instruments

The coronal waves are confidently observed with space and ground observatories, in radio band, visible lights, EUV and X-ray *etc.* The EUV imaging telescopes could well revolve the wave and oscillation activities with short cadence time and good spatial resolutions, *e.g.* Transitional Region And Coro-

nal Explorer (TRACE), Solar TErrestrial RElation Observatory (STEREO) /Extreme UltraViolet Imager (EUVI), Solar Dynamiv Observatory (SDO)/ Atmospheric Imaging Assembly

TRACE is a small satellite explorer program to investigate the dynamics of the magnetized plasma at the transitional region and corona with high temporal and spatial resolution. In the optics, the visible light is excluded from by three thin film aluminium filters, the primary and secondary mirrors are coated and optimized for one of the EUV wavelengthes, after passing the mirrors, the EUV light hits the fluorescent lumogen coating of the CCD camera. The $1\text{k} \times 1\text{k}$ CCD detector collects images over an $8.5' \times 8.5'$ field of view (FOV), filtered by one of the four normal-incidence coatings optimized for EUV and UV lights, *e.g.* 171Å (FeIX),195Å (FeXII), 1600Å(WL) *etc.* The resolution is $0.5'$ per pixel, the cadence time can be short as 10s.

EUVI is one of the five-telescope package, The Sun Earth Connection Coronal and Heliospheric Investigation (SECCHI), in the STEREO mission. It images the solar chromosphere and low corona out to $1.7R_{\odot}$ in four narrow EUV bands: 171Å (FeIX), 195Å (FeXII) *etc.* The EUV radiation is filtered at the entrance aperture by a thin aluminium filter of width 150nm, which suppresses most of UV,visible and IR radiation and screen out solar heat. Then the emissions are further selected by one of the four quadrant of the optics, the primary and secondary mirrors are coated with a narrow-band, multilayer reflective coating, optimized for one of the EUV lines. Redundant thin-film aluminium filters are placed in the optic pathway to further remove the visible and IR radiation, before the backside illuminated CCD collects the radiation and produce a image of size $2\text{k} \times 2\text{k}$ of spatial scale of $1.6'$ pixels.

SDO is launched recently under NASA's program: *Living With the Star*, to better understand the solar variabilities at small temporal and spatial scale. AIA is designed for unprecedented understanding the solar corona at the around $1.3R_{\odot}$, at multiple wavelength simultaneously, the output images will cover the whole disk of the sun with the size of $4\text{k} \times 4\text{k}$ at a resolution of 0.5 arc sec and cadence time of 10 sec or better. There are four telescopes providing 7 channels of EUV and UV lights, 4 of which provide unexplored temperature view of the sum, and 6 of which observe the ionized iron at a narrow band and cover the temperature range form 1MK to 20MK.

2 Solar Corona

Corona is also known as the upper atmosphere of the sun. According to the light sources, it is categorized into three type: K-corona, F-corona and E-corona. K-corona (kontinuierlich, German continuous) consists of continuous spectra from the scattering of free electrons, Doppler broadening of reflected absorption lines from photosphere; F-corona, Fraunhofer scatter-

ing from the dust particles; E-corona, emission lines from the corona. The corona exhibits plenty of phenomena, *e.g.* active region,coronal loops, solar plume, prominence *etc.*

2.1 Active Region

Active region is a strongly magnetized region of the sun, where the field lines extended from the photosphere into the chromosphere and corona, where the sunspots, usually occurs. Active regions emit strong X-rays and UV radiations in association of solar flares and coronal mass ejections. The active region are allocated numbers in form of AR+ four digits, by the National Oceanic and Atmospheric Administration (NOAA) of USA.

2.2 Coronal Loops

Coronal loops are well known structures of the lower corona and transition region of the Sun. They mainly emerge from chromosphere, updirected from the sunspots, and end up at foot point of opposite magnetic polarization. The coronal loops are closed magnetic flux filled with hot plasma, the plasma β is relatively small, at 0.1 or less. These plasma tube structures are very good media for the wave and oscillationary activities, *e.g.* sausage mode, kink mode, propagating waves, Alfvén waves *etc.*

2.3 Solar Plume

Solar plumes are long, feathery structures extending into the space from the poles of the sun. There are hot high-speed streams of plasma erupted from the solar plumes. Propagating compressive waves are observed in the solar plume (Deforest and Gurman [1998]).

2.4 Prominence

Prominence is a cool dense plasma structure off the solar limb, suspending from the solar surface.The temperature is much lower than the corona, The prominence extend outward in the ambient corona in large scale over time scale of several days or even months. Some of the prominences break apart and induce corona mass ejections. When the prominences are observed in the solar disk, they are called solar filaments.

3 Waves and Oscillations in the Plasma

Plasma waves and oscillations are well described by the MHD theory and are implemented in various field, *e.g.* plasma diagnostics, plasma heating *etc.* The dispersion relation for the waves is derived by introducing a perturbation of the physical parameters in equilibrium.

The ideal MHD equations include continuity equation,the momentum equation, the energy equation (adiabatic for ideal MHD), Maxwell's equations and Ohm's law (Derivations follow the context in Aschwanden [2005]),

$$\frac{D}{Dt}\rho + \rho\nabla\vec{v} = 0 \tag{1}$$

$$\rho\frac{D\vec{v}}{Dt} = -\nabla p - \rho\vec{g} + \vec{j}\times\vec{B} \tag{2}$$

$$\frac{D}{Dt}(p\rho^{-\gamma}) = 0 \tag{3}$$

$$\nabla\times\vec{B} = \mu_0\vec{j} \tag{4}$$

$$\nabla\times\vec{E} = -\frac{\partial\vec{B}}{\partial t} \tag{5}$$

$$\nabla\cdot\vec{B} = 0 \tag{6}$$

$$\vec{E} = -\vec{v}\times\vec{B} \tag{7}$$

$$\tag{8}$$

The MHD equations are rewriten by introducing the sound speed $c_s^2 = \gamma p/\rho$, and $\nabla\cdot p = c_s^2\nabla\cdot\rho$, the parameters are reduced to ρ,$\vec{v}$, and $\vec{B}$

$$\frac{D}{Dt}\rho + \rho\nabla\vec{v} = 0 \tag{9}$$

$$\rho\frac{D\vec{v}}{Dt} = -c_s^2\nabla\rho - \rho\vec{g} + \frac{1}{\mu_0}[-\frac{1}{2}\nabla B^2 + (\vec{B}\cdot\nabla)\vec{B}] \tag{10}$$

$$\frac{\partial\vec{B}}{\partial t} = -\vec{B}(\nabla\cdot\vec{v}) + (\vec{B}\cdot\nabla)\vec{v} - (\vec{v}\cdot\nabla)\vec{B} \tag{11}$$

Considering the first order perturbations of each quantity:

$$\begin{aligned}\rho(\vec{x},t) &= \rho_0 + \rho_1(\vec{x},t)\\ \vec{v}(\vec{x},t) &= \vec{v}_1(\vec{x},t)\\ \vec{B}(\vec{x},t) &= \vec{B}_0 + \vec{B}_1(\vec{x},t)\end{aligned}$$

Assume that homogeneous magnetic field is only in z-direction, $\vec{B}_0 = (0,0,B_0)$, the associated Alfvén speed $v_A = B_0/\sqrt{\mu_0\rho_0}$, and neglecting the large scale gravitational term $(-\rho_0\vec{g})$. Combining these equations into,

$$\frac{\partial^4\nabla\cdot\vec{v}}{\partial t^4} - (c_s^2 + v_A^2)\frac{\partial^2}{\partial t^2}\nabla^2\nabla\cdot\vec{v} + c_s^2 v_A^2\frac{\partial^2}{\partial z^2}\nabla^2\nabla\cdot\vec{v} = 0 \tag{12}$$

In order to obtain the dispersion relation, the perturbations is expressed in Fourier components, in form of harmonic spatio-temporal function, $\exp[i(\vec{k}\vec{x} - \omega t)]$, For the fast and slow magnetic-acoustic waves

$$\omega^4 - k^2((c_s^2 + v_A^2))\omega^2 + k_z^2 k^2 c_s^2 v_A^2 = 0 \tag{13}$$

The solutions are much dependent on the initial condition, the relative magnitude of sound and Alfvén speed, According the phase speed of the solutions, the waves are referred as fast mode wave for larger phase speed and slow mode waves for small ones. Another important factor strongly influencing the solutions is the plasma structures: plasma slab, plasma cylinder *etc.* There are good models for solar feature, the plasma cylinder is a very good model of corona loops, which will be covered in the following section.

4 Standard Model: Straght Plasma Cylinder

The magnetic cylinder is believed to model well the coronal loops, and extended in geometry to suit the filaments and solar plumes. The standard model is a simple straight cylinder of plasma, of which the internal and external parameters are different, but of cylindrical symmetry. The interior is filled with plasma of density ρ_0, pressure p_0 in a magnetic field of $B_0\hat{z}$. The associated sound speed, Alfvén speed and tube speed are defined respectively as $C_{s0}^2 = \gamma p_0/\rho_0$, $C_{A0}^2 = B_0^2/(\mu_0/\rho_0)$, $C_{T0}^2 = C_{s0}^2 C_{A0}^2/(C_{s0}^2 + C_{A0}^2)$, while the exterior is the ambient plasma of density density ρ_e, pressure p_e in a magnetic field of $B_e\hat{z}$. The corresponding sound speed, Alfvén speed and tube speed are $C_{se}^2 = \gamma p_e/\rho_e$, $C_{Ae}^2 = B_e^2/(\mu_0/\rho_e)$ and $C_{Te}^2 = C_{se}^2 C_{Ae}^2/(C_{se}^2 + C_{Ae}^2)$. The boundary condition requires to balance the total pressure or the displacement.

$$p_0 + \frac{B_0^2}{2\mu_0} = p_e + \frac{B_e^2}{2\mu_e}\xi_{r0} = \xi_{re} \tag{14}$$

The derivation of the dispersion relation is based on linearisation of the MHD equations and the first order differential equation, perturbed at equilibrium condition with a $\delta P_{tot}(r)\exp[i(k_z z + m\phi - \omega t)]$, (Sakurai et al. [1991], Nakariakov and Verwichte [2005])

$$D\frac{d}{dr}(r\xi_r) = (C_s^2 + C_A^2)(\omega^2 - C_T^2 K_z^2)(\kappa^2 + \frac{m^2}{r^2})r\delta P_{tot} \tag{15}$$

$$\frac{d}{dr}(\delta P_{tot}) = \rho_0(\omega^2 - C_A^2 k_z^2)\xi_r \tag{16}$$

$$-\frac{im}{r}\delta P_{tot} = \rho_0(\omega^2 - C_A^2 k_z^2)\xi_\phi \tag{17}$$

where the ξ_r and ξ_ϕ are perturbations displacement in the radial and azimuthal directions. The parameters D and κ are defined as

$$D = \rho_0(C_s^2 + C_A^2)(\omega^2 - C_A^2 k_z^2)(\omega^2 - C_T^2 k_z^2) \tag{18}$$

$$\kappa^2(\omega) = -\frac{(\omega^2 - C_s^2 k_z^2)(\omega^2 - C_A^2 k_z^2)}{(C_s^2 + C_A^2)(\omega^2 - C_T^2 k_z^2)} \tag{19}$$

The second and third equations can be rewritten as

$$(\omega^2 - C_{A\alpha}^2 k_z^2)[\frac{d^2}{dr^2} + \frac{1}{r}\frac{d}{dr} - (\kappa_\alpha^2 + \frac{m^2}{r^2})]\delta P_{tot} = 0 \tag{20}$$

The first term describes the Alfvén wave, the second term gives the solution of fast and slow mode magneto-acoustic waves. Solve the equation by applying the boundary conditions, namely balancing total pressure and radial velocity, and obtain,

$$\rho_e(\omega^2 - C_{Ae}^2 k_z^2)\kappa_0 \frac{I_m^{'}(\kappa_0 a)}{I_m(\kappa_0 a)} - \rho_0(\omega^2 - C_{A0}^2 k_z^2)\kappa_e \frac{K_m^{'}(\kappa_e a)}{K_m(\kappa_e a)} = 0 \qquad (21)$$

where I_m and K_m are modified Bessel functions of order m, the parameters κ_e and κ_0 are the transverse wave numbers in the external and internal media.

For the body modes that oscillate in the tube and are evanescent outside, the conditions $\kappa_e^2 > 0$ has to be fulfilled. Assuming that $\kappa_{e,0} > 0$, the parameter determines the oscillationary mode of the waves, waves with $m = 0$ are *sausage* mode, those with $m = 1$ are *kink* mode, those with higher m are referred as *flute* or *ballooning* modes.

5 Propagatingclearly Perturbation of Intensity

The discussions of MHD waves of previous sections implicitly mean standing waves, in which case the footpoints of the coronal loops anchored at the chromosphere, the oscillations are normally damped after several oscilation periods, however, when the trigger or source occurs at one of the footpoints, the wave is damped before reflection at the other node and merging into standing mode. This kind of mode is referred as propagating MHD wave. After the launch of SOHO and TRACE, the observations confirm the existance of propagating waves, this includes the discovery of compressible waves in polar plumes (Deforest and Gurman [1998]), wave trains in coronal loops (Berghmans and Clette [1999], De Moortel et al. [2002a,b], De Moortel [2009])

The propagating slow-mode MHD waves are well described in both theory and are supported strongly by observations. The evolutionary equation for slow MHD wases was derived by Nakariakov et al. [2000] from viscous MHD equation:

$$\frac{\partial \rho}{\partial t} + \frac{\partial}{\partial s}(\rho v) = 0 \qquad (22)$$

$$\rho(\frac{\partial v}{\partial t} + v\frac{\partial v}{\partial s}) = -\frac{\partial p}{\partial s} - g\rho + \frac{4}{3}\eta_0 \frac{\partial^2 v}{\partial s^2} \qquad (23)$$

$$\frac{1}{\gamma - 1}(\frac{\partial p}{\partial t} - \frac{\gamma p}{\rho}\frac{\partial \rho}{\partial t}) = \frac{\partial}{\partial s}(\kappa_{\parallel}\frac{\partial T}{\partial s}) \qquad (24)$$

where s is the loop lenth coordinate, $\rho(s)$, $v(s)$, $p(s)$, $T(s)$ are plasma density, longitudinal speed, plasma pressure, and plasma temperature. γ is the

adiabatic index, $\kappa_{\shortparallel} = \kappa T^{5/2}$ is the thermal conductivity along the magnetic field, η_0 is the compressive viscosity coefficient, and $g(s)$ is the gravitational acceleration along the loop coordinate s,

$$g(s) = g_{\odot} \cos(\frac{s}{r})(1 + \frac{r}{R_{\odot} \sin(\frac{s}{r})})^{-2}.$$

The above equations lead to modified Burger's equation, which can be solved by introducing Fourier components,

$$\frac{\partial v}{\partial s} - \frac{v}{2\lambda_n} + \frac{\gamma + 1}{2c_s} v \frac{\partial v}{\partial \xi} - \frac{R_{\odot}\rho_0(0)\bar{\eta}}{2\rho_0(s)} \frac{\partial^2 v}{\partial \xi^2} = 0 \tag{25}$$

$$v(s) = v(0) \exp[\int_0^s (\frac{1}{2\lambda_n(x)}) - \frac{R_{\odot}\rho_0(0)\bar{\eta}k^2}{2\rho_0(x)} dx] \tag{26}$$

where $\xi = s - c_s t$ is the comoving coordinate in the sound speed frame, $\lambda_n(s) = c_s^2/(\gamma g)$ is the local density scale height, $k = \omega/c_s$ is the wave number, and $\bar{\eta}$ is defined as

$$\bar{\eta} = \frac{1}{\rho_0(0) c_s R_{\odot}} [\frac{4\eta_0}{3} + \frac{\kappa_{\shortparallel}(\gamma - 1)^2}{R_{\rm gas}\gamma}].$$

The slow-mode MHD waves were observed a lot in multiple wavelenghs with various instruments (see Table-1). The typical speed are measured lower than the acoustic speed at coresponding temperature, as measurements were subjected to the projection effect along the line of sight. The method to detect the signal of propagating intensities is proposed in Deforest and Gurman [1998]. The EUV emission flux profile $F(s,t)$ along the loops is first extracted from the images or datatube, normally, the integral average should be taken to suppress the random noise, either constant pixels wide along the loop structures or the average of the cross-sections within the diffuse coronal structures. Then contour image of $F(s,t)$ is ploted with s and t as axises, this is called a time-distance plot, in which the ripple patterns are visible. With time-distance plot, the maximum of the intensity envelop at each location s is measured, a linear fitting of the peaks will give the propagating speed of the wave (Fig.1, King et al. [2003]). King et al. [2003] reported a two wavelenghs study (171Å and 195Å) of propagating slow wave, the measured periods by wavelet method and estimated speeds are reported to be $2-3$ mins and $5-8$ mins, and $150-190$km/s, respectively, while the mean sound speeds are, for 171Å, $c_s \approx 147$km/s at $T \approx 1.0$MK, for 195Å, $c_s \approx 180$km/s at $T \approx 1.5$MK. These results are well consistant with the theory. There is another way to visualized the propagating feature clearly, by ploting the running diffrence plot, namely $F(s,t) - F(s, t - \Delta t)$, in which case the diagnoal ridges are clearly indentified, the measurement of the slopes will give the propagating speed (Fig.2, De Moortel et al. [2000]).

The estimated period and speed are $180 - 420$ seconds and $70 - 165$km/s (see Table-1).

The obervations of polar plumes were reported by Deforest and Gurman [1998], which is summarized in the appendice. The recent advances, including the the link with other studies in chromosphere and transition region, were reviewed by De Moortel [2009], also summarized in the appendice.

Table 1: Overview of slow MHD waves observated in coronal structures, N is the number of event, adapted from Aschwanden, Physics of the Solar Corona, chapter 8, p.334 and De Moortel 2009

Observer	N	Wavelength(s)	Speed v[(km/s)]	Instrument
DeForest & Gurman (1998)	1	171Å	$\approx 75 - 150$	SoHO/EIT
Berghmans & Clette (1999)	3	195Å	$\approx 75 - 200$	SoHO/EIT
Nightingale *et al.*(1999)	1	171Å, 195Å	$\approx 130 - 190$	TRACE
Schrijver *et al.*(1999)	1	195Å	$\approx 70 - 100$	TRACE
De Moortel *et al.*(2000)	1	171Å	$\approx 70 - 165$	TRACE
De Moortel *et al.*(2002a)	38	171Å	122 ± 43	TRACE
De Moortel *et al.*(2002b)	4	195Å	150 ± 25	TRACE
Robbrecht *et al.*(2001)	4	171Å,195Å	$\approx 65 - 150$	EIT, TRACE
Berghmans *et al.*(2001)	1	171Å,195Å	$\cdots$	EIT, TRACE
Sakurai *et al.*(2002)	1	5303Å	≈ 100	Norikura
King *et al.*(2003)	1	171Å, 195Å	$\approx 150 - 190$	TRACE
Marsh *et al.*(2003)	1	171Å, 368Å	$\approx 50 - 195$	CDS, TRACE
McEwan & De Moortel (2006)	25	171Å	98 ± 6	TRACE

6 Current Projects

My currently project is to study the slow-mode propagating MHD waves, focusing on the spatial variation and correlations and long period behaviors, especially the 3mins oscillation. The images of size 512×512 are taken by TRACE in two bandpasses 171Å and 195Å. The whole observation program lasts for around 5days, from 31 - Jun - 1998 UT 00:00.000 to 04 - Jul - 1998 UT 23:59.999, the data are mostly continuous observations, except some routine pointing to the solar limb for about half a hour to one hours. Very good propagating waves are clearly seen by eye.

The dataset from TRACE in FITS file are first prepared by using the IDL routine in SolarSoft, TRACE_PREP, calibrations are done by implementation of this procdure, optional key word are added: /wave2point_corret, the images pointings are aligned to the reference wavelength, which are assured to be correct; /unspike, /destreak: the spike and streaks from radiation belt and cosmic ray are removed; /deripple will remove the readout noise of the

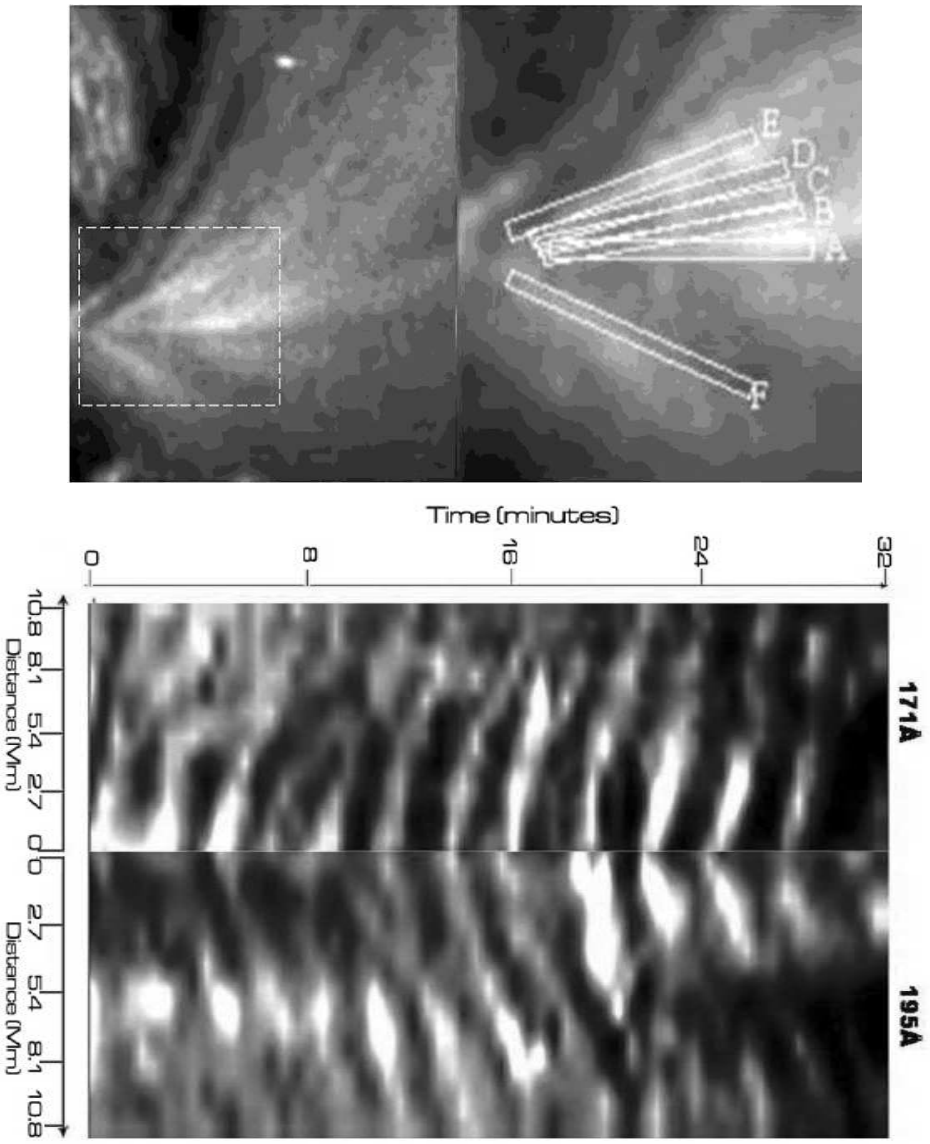

Figure 1: Top left panel: active region AR8253, imaged by TRACE on 2 July 1998 UT 06:00 in the 195Å bandpass. Top right panel: the slits analysed, where apparen propagating intensities are observed. Bottom panel: The time-distance plot of along slit A marked in the top-right panel, the time-distance plots of both bandpass 171Å and 195Å are placed in parallel, but opposite direction. King et al. [2003]

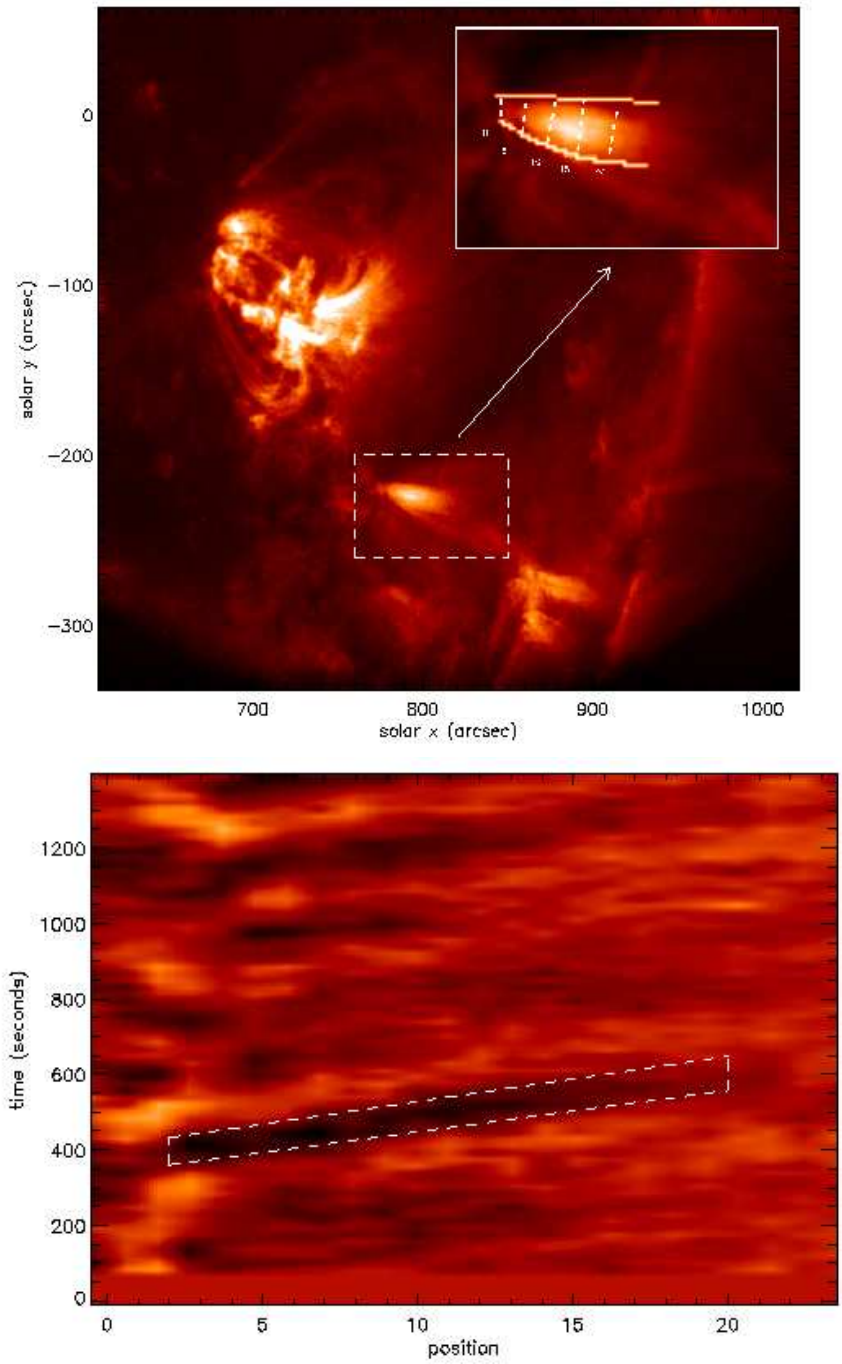

Figure 2: Top panel: the active region AR8496, observed by TRACE 171Å at 24-Mar-1999 UT 06:47, subimage on the top-right is the area supporting the propagating intensities. Bottom panel: the running diffrence of the region indicated on the top image, the positions are pixel index, rather than the real position, a clear ridge is visible, the periods and propagating speed are measured to be $180 - 420$ seconds and approximately $70 - 175$km/s, respectively. De Moortel et al. [2000]

CCD, /normalize keyword will normalize the output image to the exposure time into DN per second, as the exposure times are subjected to slight variation, and the CCD response signals are found to be linear proportional to the exposure time; /float will give the output images in float value for each pixels, rather than intergers, which will increase the storage size of the images, however, this will facillitate further processing to an enhanced preciseness.

The next step that have been done is to trace the target in the images as precise as possible. The active regions in the images are in different locations due to multiple effect. It is co-rotating with the solar surface, and axis of the sun is also gyrating in long period, *e.g.* days . The spacecraft repointed frequently to include the target in the image range $8.5' \times 8.5'$, the spacecraft is subjected to slight pointing drift, which is negligible for short duration less than hours, but is rather severe for long period of observation. The dataset is of size data(nx, ny, nt), where nx and ny are the numbers of pixels in x and y axis, nt is the time index of the images. For two images with center of view $(XCEN(0), YCEN(0))$ and $(XCEN(1), YCEN(1))$, the repointing is denoted as $D = (D_x, D_y) = (XCEN(1) - XCEN(0), YCEN(1)) - YCEN(0)$, The solar differential rotations is calculated as $R = (R_x, R_y)$, (NB. $R_y \neq 0$ is due to the gyrating of the rotating axis), then the sub dataset of size subdata$(x_1 - x_0 + 1, y_1 - y_0 + 1, nt)$ is extracted by

$$\text{subdata} = \text{data}[(x_0 - D_x + R_x) : (x_1 - D_x + R_x), (y_0 - D_y + R_y) : (y_1 - D_y + R_y), *]$$

The region of interest is tracked by considering spacecraft re-pointing and solar rotation, the uncertainties of the solar rotational model and spacecraft pointing drifts are minimized by correlations. The displacements of the images are coalign with the reference image by shifting an offset calculated by cross-correlation with the reference image. The sub dataset, after this step are ready for further analysis. The images from sub dataset are then displayed in the movie co-rotating with the solar surce, D_x pixels away from the reference image.

A slit is extracted from the data to form a time-distance plot as in top panel of Fig.3. Wave patterns are visible in the image. For each pixel, the intensity are interpolated into a new evenly spaced datacube of the same size, as Fast Fourier Transform (FFT) requires strict evenness of the time series, the original sampling times are subjected to slight variation due to various exposure time. After FFT, a filter is apply to the signal in frequency doman, optionally *ideal* or *gaussian* , with the selected frequency near the centre of the window. Then the time series are sythesized with the average value subtracted, which are illustrated in the bottom of the bottom panel, as shown in Fig.3. Two ideal filters of frequency band $[0.005, 0.006]$Hz including $1/180\text{s} = 0.0056$Hz and $[0.003, 0.004]$Hz embraing $1/300\text{s} = 0.0033$Hz are applies to the time series. The restored time-distance plot are show in Fig.

3.These two ideal filters are also apply to the movie, pixel by pixel, then each pixels should oscilate independently with one another with random phase and amplitude if there is no collected behaviors, however if propagating slow-mode wave exist, the involved pixels are modulated and apparent propagating intensity can be observed. The resulting movie confirm this point, in the movie filtered by 3-min filter, the propagating intensity are clearly visible, while it vanishes after filtered by the ideal 5-min filter.

7 Future Plan

7.1 Shot Term Plan: April - June 2010

From April to the end of June, I will focus on the slow-mode magneto-acoustic waves, to study its long period evolution of the parateters, *e.g.* stability of the phase, evolution of the period and propagating speed, and other features. The procedures to analysis the data were already developed, and the wave patterns are recognized with the time-distance plot, the next step is to obtain the parameters, with data analysis technique, *e.g.* periodogram, windowed FFT, wavelet *etc.* These can be done in a short time, since the data are already processed at good stage and the procedures are available, either developed within the group or on the website well acknowledged.

The result of current study will have to be abstracted and submitted to the BUKS 2010 (Belgium, United Kingdow, Spainn) meeting at St Andrews University at the end of April: *Workshop on MHD waves and seismology of the solar atmosphere*. The formal submission to a referred journal will be expected at the end of June.

7.2 Long Term Plan: July - December 2010

After the completion of the first project, it is expected that the data from the recently launched SDO/AIA is almost available for the solar community. The next project will be much involved with the advanced instrument.

- Jun-Oct: After the initial internal test and software development, the data should be available on the NASA website. The initial task is to get familarized with the AIA pre-processing software, and to start analyzing the similar phenomena, *e.g.* slow mode MHD waves, sunspot events with the multi-channel telescopes, the main focus will be still in the active region and magnetic field dynamics. However if there are new discoveries beyond the current knowledge level, we will focus on that. In July or August, another data updating meeting will be held, the feedback will somehow help with the project.

- Oct-Dec: The second project will be formally concepted, which depends on the advances made by SDO/AIA. I alread gain experience

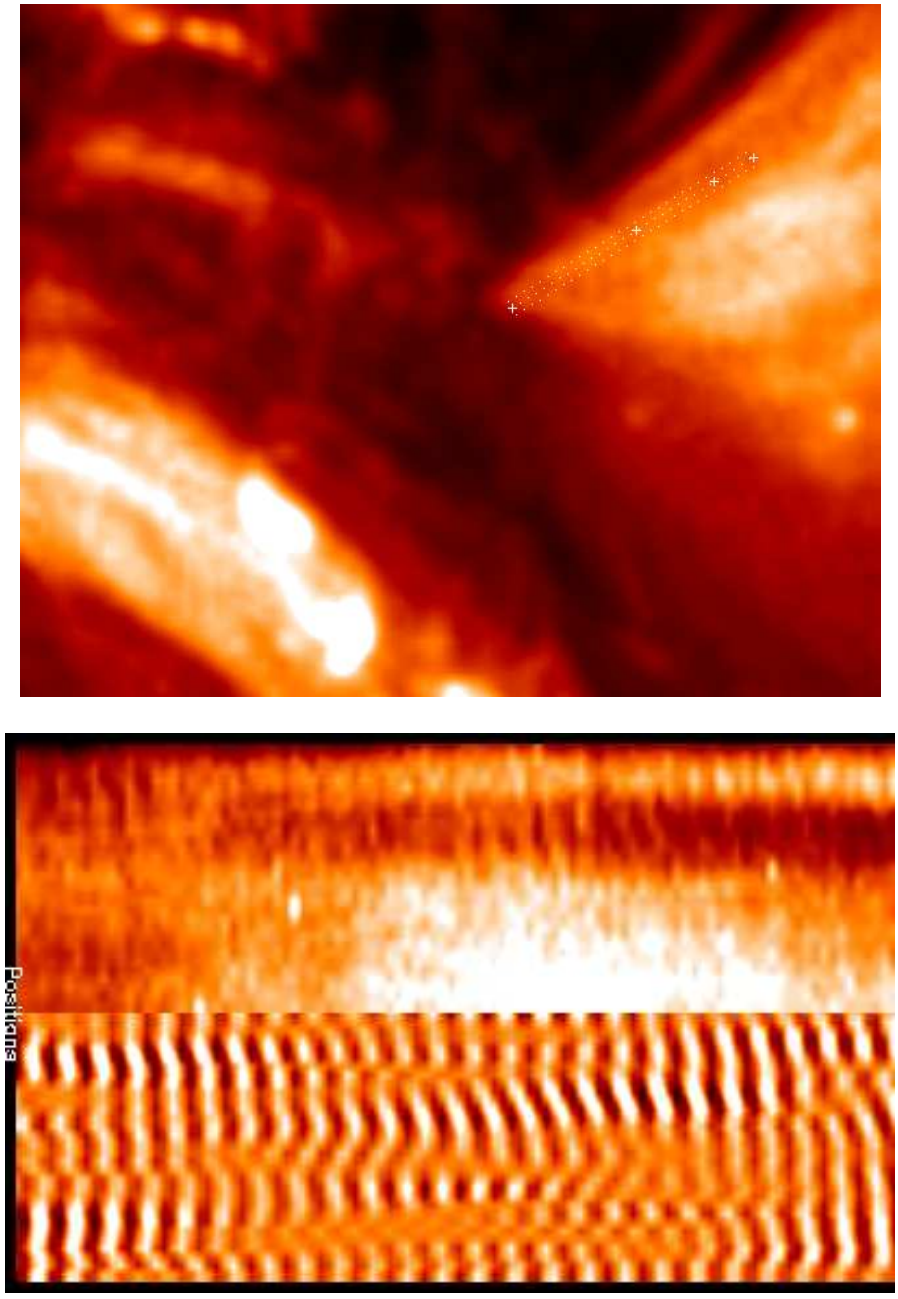

Figure 3: Top panel: The typical image taken by TRACE in 171Å bandpass at 03 - Jul -1998 UT 00:00, the coronal structure is a diffuse corona, the slit analyzed are maked with dots. Bottom panel: The time distance plots are stacked in parallel, top one from the original dataset and bottom one filtered in a narraw ideal rectangular window of period embracing 3mins. Clear ripple patterns are seen from both time-distance plots, especially the ideally filtered one. As the time duration for plots are around 2 hours, the ripples looks like vertical, however, they are the same as in King et al. [2003], if they were plotted in the same time scale.

from current project and initial familarization with the the AIA software. It will take less time to obtain output from the project, the result are expected for journal submission before Chrismas.

- Backup: If due to some reason, SDO/AIA is not available, we will shift to Nobeyama Rodia Observatory, which is not worth to discuss in detail at the current stage.

7.3 Year 2 and 3

Since there exists a risk of the availability of SDO/AIA, The longer plan is subjected to large uncertainties, it not realistic to make one, after the initial analysis of the AIA data for reliabilities and possible break events, a longer plan should be make in Oct 2010, which will be included in the next progress report and reseach plan.

References

M. J. Aschwanden. *Physics of the Solar Corona. An Introduction with Problems and Solutions (2nd edition)*. December 2005.

D. Berghmans and F. Clette. Active region EUV transient brightenings - First Results by EIT of SOHO JOP80. , 186:207–229, May 1999.

I. De Moortel. Longitudinal Waves in Coronal Loops. *Space Science Reviews*, 149:65–81, December 2009. doi: 10.1007/s11214-009-9526-5.

I. De Moortel, J. Ireland, and R. W. Walsh. Observation of oscillations in coronal loops. , 355:L23–L26, March 2000.

I. De Moortel, A. W. Hood, J. Ireland, and R. W. Walsh. Longitudinal intensity oscillations in coronal loops observed with TRACE II. Discussion of Measured Parameters. , 209:89–108, September 2002a. doi: 10.1023/A:1020960505133.

I. De Moortel, J. Ireland, R. W. Walsh, and A. W. Hood. Longitudinal intensity oscillations in coronal loops observed with TRACE I. Overview of Measured Parameters. , 209:61–88, September 2002b. doi: 10.1023/A:1020956421063.

C. E. Deforest and J. B. Gurman. Observation of Quasi-periodic Compressive Waves in Solar Polar Plumes. , 501:L217+, July 1998. doi: 10.1086/311460.

D. B. King, V. M. Nakariakov, E. E. Deluca, L. Golub, and K. G. McClements. Propagating EUV disturbances in the Solar corona: Two-wavelength observations. , 404:L1–L4, June 2003. doi: 10.1051/0004-6361:20030763.

V. M. Nakariakov and E. Verwichte. Coronal Waves and Oscillations. *Living Reviews in Solar Physics*, 2:3–+, July 2005.

V. M. Nakariakov, E. Verwichte, D. Berghmans, and E. Robbrecht. Slow magnetoacoustic waves in coronal loops. , 362:1151–1157, October 2000.

T. Sakurai, M. Goossens, and J. V. Hollweg. Resonant behaviour of MHD waves on magnetic flux tubes. I - Connection formulae at the resonant surfaces. , 133:227–245, June 1991. doi: 10.1007/BF00149888.

Appendices

A Nakariakov and Verwichte (2005)

Waves and oscillations of the solar corona are well observed with modern instruments and are believed to the promising candidate in explaining the dilemma of corona heating and acceleration of fast solar winds. Combining the observations and MHD wave theory, the physical parameters, *e.g.* magnetic field, transport coefficients, fine-structure and heating function are established, this is called MHD seismology. Corona waves and oscillations, including the newly developed MHD seismology are discussed in this review paper in the series of *Living Review of Solar Physics*.

A plasma structure − straigh cylinder, which is a good model of corona loops, is introduced and, further, the dispersion relation with linearization of the MHD equation under harmonic perturbation to the total presure $\delta P_{tot}(r)\exp[i(k_z z + m\phi - \omega t)]$. For the modes that are evanescent outside the cylinder. The dispersion relation was three groups of solution: Alvén wave, fast and slow mode waves. The waves is further referred to as sausage modes ($m = 0$), kink modes ($m = 1$) and flute or ballooning modes ($m > 1$)

A typical kink oscillation of coronal loops was observed with TRACE spacecraft in the AR8270 on 14 July 1998 by Nakariakov *et al.*1999. By fitting the loop time − displacement plot, The period and decay time was found at $P = 4.3 \pm 0.9$min and $\tau = 14.5 \pm 2.7$min. Assuming a density ratio of $\rho_e/\rho_0 = 0.1$, the magnetic field strength is estimated

$$B_0 = \sqrt{\mu_0 \rho_0} C_{A0} \approx \frac{\sqrt{2\mu_0} L}{P} \sqrt{\rho_0 (1 + \rho_e/\rho_0)}$$

whereμ_0 is the magnetic permeability constant L is the length of the loop,C_{A0} is the internal sound speed.

Propagating slow waves, moving at the speed of sound, were first observed in coronal holes by Ofman *et al.*(1997) with SOHO/UVCS, and at solar plume by DeForest and Gurman (1998). As the sound speed is a function of temperature and adiabatic index γ, the measured speed, subjected to projection effect, can serve a tool for coronal seismology. The decreasing correlation coefficients along the structure suggested that there might be a substructure of the active region, which cannnot be resolved with current instruments. Future studies are very promising to investigate more details, 3D observations to compensate the projection effects, and higher temporal and spatial resolutions to dig the possible speed variations and finer structures.

The observation of propagating fast waves is limited by current available instruments. Since the period and wavelength of fast waves couldn't be well resolved by the cadence time and resolution of the detectors. Williams *et al.* (2001,2002) and Katsiyannis (2003) reported the observations of rapidly

propagating compressive wave trains in the coronal loops with SECIS. The estimated speed is about 2100km/s with a mean period of 6 s in a quasi-periodic pattern. The measurement of amplititude agreed well with theoretic model (Nakariakov *et al.*(2003)), however, the large uncertainties limited further analyisis. Verwichte *et al.*reported the direct observation of clear transverse fast wave and interpreted as fast magnetoacoustic kink wave. The study was performed with TRACE 195Å at a hot supra-arcade above post-flare loop arcade. The wave periods and wavelengths were estimated in the range of $90 - 220$s and $20 - 40$Mm respectively. The plasma slab structure was more suitable than cylindrical model in order to explain the observations.

Current observations are very much limited by the availibilities of good instrument. With the launch of SDO, the AIA detector will send by images of the whole sun of size $4\text{k} \times 4\text{k}$ with cadence time 3s and resolution of $0.5'$, which could boost the activities and complement current knowledge of the waves.

B De Moortel (2009)

This paper is an updated review of propagating intensity disturbances in quiescent coronal loops that are intensively studied recently, a further extension of another two reviews in 2002, which focus more on the detections of oscillations, measurements of physical paramenter, statistics of the feature distributions and metheds of data analyisis. While in this one, more efforts were concentrated on physical and interpretions of the damping features, apparent links to other observations and modellings in the chormosphere and transitional regions, possible triggerring mechanism (*e.g.* globlal solar 5-min p-mode oscillations, leakage from inclined magnetic portals) of the propagating oscillations.

The propagating intensity perturbations are found to be quasi-periods and persist for 5 cycles in a wave-train sequence at the period of about 3 mins above sunspot umbras and around 5 mins at off-sunspot regions. Theoretical modelling indicated that dissipation causes decay of the perturbation amplititude, while the effects of gravitirional stratification is the reverse. Further modellings were performed by De Moortel et al. (2004) with inclusion of thermal conduction, compressive viscosity and optically thin radiation, and found the thermal conduction is the main contributor, while the impacts of the latter two is negligible. The modellings was extended by considering area divergence and gravititional stratification, and was concluded that the combination of thermal conduction and area divergence can account for the observed damping.

Recent studies, both theoretical and observational, show that the inclination of magnetic field could provide magnetic portals and allow the globlal

5 min p-modes leak into the corona. At sunspot umbras, the near-vertical magnetic fields reflects back the 5-min p-modes, thus 3-min perturbations are dominating, while at plage region (non-sunspot), the inclined magnetic fields are not able to cut-off the 5-min p-modes, so the global surface 5-min p-modes can be observed clearly.

Both upward and downward flows are observed with Hinode / XRT and Hinode/ EIS near the edges of active regions with Doppler shifts techniques. The speeds of the outflows are found up to 100km/s close to local sound speeds (corrected by projection effections), and behaves similarly to propagating intensity, while non study annouces wave pathern along the flows, so it is worhwhile to investigate this link with high spatial and temperal resolutions.

C Torrence and Compo (1998)

This paper submitted by C. Torrence and G.P. Compo, with its code in FORTRAN,C,and IDL, is good practical step-by-step guide to wavelet analysis, with the example from the time series of the El Niño Southern Oscillation (ENSO). the Edge effects due to finite time series beared with Windowed Fourier Transform are inherited by wavelet transform and are discussed and illustrated in the samples. The selections of wavelet functions are based on the features of the time series, complex wavelets for oscillations (This is good selection for analysis of waves and oscillation) and real-valued wavelets for those containing singular frequencies components. The significance level and confidence intervals are calculated with both white and red noises. The techniques to improve the quality of analysis are given, such filtering , cross-wavelet spectra etc.

This is a very good guide for obtaining oscillation components confidently from the time series of solar data. The procedures on their website can be modified slightly and implemented in short time, A very good colourful figures can be produced quickly at publication level. The only flaw is that the codes are only ready for evenly-spaced time series, normally the solar datum are semi-even in short period and un-even in long observation, namely, the observations were made almost in the same intervals with slight variations of exposure time, and were oriented for other observations, or closed for maintenance, or to avoid strong radiation belts to protect the instruments, routinely during the day and year periods. So for short observations (several minutes to several hours), interpolation of the time series to even time intervals is well acceptable, while for long time series with data gaps, other techniques for unevenly-spaced time series must be implemented, such as Lomb-Scargle method (which is also one of the key texts reviewed).

D Scargle (1982)

The periodogram is a commomly used spetral analysis technique to extract periodic compoment from unevenly spaced data. Other spetral analysis tool are not so efficient, e.g. FFT, wavelet, as unevenly spaced data might generate spurious periods equal to time gaps or their harmonics in the FFT or DWT, however periodogram is able to avoid such incapablities, and it is equivalent to least-fit of sinusoids to the data.

In this paper, the reliability and efficiency of periodogram is studied. A modification of the classic definations (see Eq. below) is made to retain the staticstic behavior and more suitable for numerical realizations, upon which most of the available codes are based. The staticstical analysis is elaborated with the inclusion of expressions for false alarm rate and detection efficiency. $P_X(\omega)$ is the distribution probability of frenquency compoment ω, defined as,

$$P_X(\omega) = \frac{1}{2}\{\frac{[\sum_j X_j \cos\omega(t_j-\tau)]^2}{\sum_j \cos^2\omega(t_j-\tau)} + \frac{[\sum_j X_j \sin\omega(t_j-\tau)]^2}{\sum_j \sin^2\omega(t_j-\tau)}\}$$

where X_j is a physical observable at time series t_j, τ is defined as

$$\tan(2\omega\tau) = \left(\sum_j \sin 2\omega t_j\right) / \left(\sum_j \cos 2\omega t_j\right)$$

The codes for periodogram analysis are available in various formats, also our own procedures in IDL (Nakariakov). I will use the routines in IDL to analize the time series extracted from the solar EUV emissions or other time series in the future. The routine has to be improve to provide more flexibility and clearance.

E DeForest and Gurman (1998)

Slow-mode waves were first observed in the solar polar plume (open field structure, in contrast to closed structure or coronal loops). With the data in 171Å bandpass from SOHO/EIT, DeForest and Gurman (1998) found filamentary substructure, on a scale of $5''$, oscillating on the time scales of several minutes in wave trains of $10-15$mins periods. The propagating speeds were estimated at $75-150\mathrm{kms}^{-1}$. The quasi-periodic perturbations to the overall intensity of the plumes amounts to $10\%-20\%$. The energy flux carried by the waves was calculated to be $150-400\mathrm{Wm}^{-2}$ by assuming the waves to be sonic, it is not sufficient to heat the coronal holes, which is about $1\mathrm{kWm}^{-2}$ (Parker 1991).

Besides the new observations, another contribution of the paper is that a well accepted procedure to prepare the data for analysis, which is a preliminary stage for my future work, was established. Besides the normal

steps, like removing the spikes,JPEG compression artifacts, cosmic rays and streaks in the dataset, exposure normalization, background subtraction, feature tracking, and evolution chart are worth performing in order to improve the quality of the data and avoid missing information.

In the solar data from the spacecraft, the raw images are subjected to global brightenings and dimmings, it is originated from the small variations of exposure time. A correction should be made in order to remove the offsets. By interpolating from the response function of the detector to the exposure time, which is usually linear, the intensities of the images are excluded from this effect by scaling each pixel by the response function.

In order to increase the contrast of the objects from the background, it is always useful to subtract the background corona from the images. A radial background model corona was generated: the minimal values of the pixels along the curves concentric with the solar centre was founded as a functions of radius from disk centre, and smoothed over 10 bins along the radial directions. Then the spherically symmetric background corona was subtracted from the scaled images.

To track the features in the images, the rotation of the sun should also be removed, if itself is not the objects for analysis. A solar rotational model is incorporated, (The following is not included in this paper) the common one is synodic using the Allen quantities. there are also uncertainties introduced by the solar rotational model and possible spacecraft pointing drifts, which can be further minimized by correlation methods.

To see the intensity perturbation features, a time-distance technique is implemented. A time-distance plot is to take the intensities of the pixels along certain curve and stacked in the time sequence. The perturbation features can be observed from the time-distance plot. The propagating of the waves and the speeds are investigated by generating the running difference plot, in which the intensities of the points have to be subtracted from those of 6 minutes ahead, if not available, interpolation is made from the nearby frames.

These steps are worth trying if the signal-to-noise (S/N) is not good enough, however it is not necessary to follow all of them, some can be avoided. *e.g.* for short period, solar rotation is negligible and can be skipped, background subtraction can be also avoided if the S/N is good enough.